ISSN 1063-7826, Semiconductors, 2007, Vol. 41, No. 2, pp. 190–196. © Pleiades Publishing, Ltd., 2007.
Original Russian Text © A.E. Galashev, I.A. Izmodenov, A.N. Novruzov, O.A. Novruzova, 2007, published in Fizika i Tekhnika Poluprovodnikov, 2007, Vol. 41, No. 2, pp. 196–202.

Computer Study of Physical Properties of Silicon Nanostructures

A. E. Galashev[a]^, **I. A. Izmodenov**[b], **A. N. Novruzov**[b], **and O. A. Novruzova**[b]
[a]*Institute of Thermal Physics, Ural Division, Russian Academy of Sciences, Yekaterinburg, 620016 Russia*
^e-mail: galashev@ecko.uran.ru
[b]*Institute of Industrial Ecology, Ural Division, Russian Academy of Sciences, Yekaterinburg, 620219 Russia*

Submitted May 31, 2006; accepted for publication June 29, 2006

Abstract—The method of molecular dynamics is applied to the study of variations in the physical properties of vitreous and amorphous silicon nanoparticles when heated from 300 to 1700 K. The nanoparticles consist of 300, 400, and 500 atoms. The energy and the average length of the Si–Si bond are calculated, and the average number of bonds per atom is determined. Thermally induced strains tend to change the distribution of the excess potential energy among the concentric layers in the nanoparticles. It is shown that, energetically, the most preferential layer is the middle spherical layer of the "warm" nanoparticle. The temperature behavior of the radial and tangential components of the atomic mobility coefficient in the concentric layers is considered. It is established that there is a liquid layer at the nanoparticle surface in the vicinity of the transition to melting. The vitrified Si_n nanoparticles are kinetically more stable than the similar-sized amorphous particles.

PACS numbers: 61.46.Bc

DOI: 10.1134/S1063782607020157

1. INTRODUCTION

Amorphous solid materials are the subjects of extensive experimental and theoretical studies. Of the greatest interest are tetrahedral amorphous solids (*a*-Si, *a*-Ge), which have found wide use in microelectronics. Carbon, silicon, and germanium are in the same group of the periodic table and have the same diamond-like structure in the crystalline state. However, the properties of these macrocrystals are rather different. At the nano-scaled level, these crystals show substantially different behavior as well. Carbon is capable of forming fullerenes and nanotubes, while such structures are unstable in the case of silicon or germanium [1]. Computer simulations predict much worse stability of Si- or Ge-based fullerenes. According to [2], the destruction of the Si_{60} and Ge_{60} fullerenes begins at 700 and 200 K, respectively.

It has been shown that nanocrystals or amorphous nanoparticles (quantum dots) closely packed in silicon nitride or silicon dioxide can enhance the incident light [3, 4]. Such nanoparticles are often referred to as quantum dots, because their properties are in many respects similar to the properties of individual atoms. These structures can be considered as zero-dimensional quantum wells. For these wells, the energy is typically quantized at lengths several hundreds of times longer than the lattice constant. A quantum dot can be considered as a trap for electrons. Once trapped at "a dot," none of the electrons has sufficient energy by itself to escape from the dot. The smaller the quantum dot, the higher the potential energy necessary for the electron to escape from the created potential well. Quantum dots of the semiconductor crystals in use at the present time range from 1 to 10 nm in diameter, i.e., involve between 300 and 10^5–10^6 atoms.

The optical properties and electronic structure of quantum elements (dots) are crucially dependent on their size and on the atomic arrangement in the nanoparticle. For example, it is possible to vary the spectral position of the luminescence peak by varying the nanoparticle size [5]. In addition, the luminescence intensity for amorphous quantum dots is higher than that for crystalline quantum dots. Materials varying in the size of the built-in quantum dots and in atomic arrangement and structural symmetry of the nanoparticles can be used in luminescent devices, laser diodes, sensors, and switches. Such materials can be used to record and read out optical information.

In theoretical studies of these materials, a topical problem is to derive physically substantiated amorphous structures for which the theoretically obtained results can be compared to the experimental data. The thermodynamic, mechanical, and structural properties of amorphous materials can be adequately described by the Monte Carlo (MC) molecular-dynamic (MD) computer simulation. The MD simulation of germanium nanoparticles 2–3 nm in size shows that, after the nanoparticles are kept at a temperature of T = 1000 K for 1 ps and subsequently cooled to 300 K and left for relaxation for 2 ps, the nanoparticle changes its structure from the diamond-like structure, with floating bonds at the surface, to the vitreous structure, in which 5- and 6-membered rings prevail [6]. Crystalline diamond-like-structured quantum dots of the same size were derived in the computer experiment, in which the nanoparticle surface was passivated with hydrogen; as a result, the floating bonds were terminated with the hydrogen atoms. By the quantum MC and ab initio MD methods, Mitas et al. [7] found two stable forms of a Si cluster of 20 atoms: an oblong cluster formed by the two linked Si_{10} stable clusters, and a sphere-like cluster with the shape of a distorted dodecahedron. Among the somewhat bigger clusters, the Si_{45} isomers derived by the ab initio MD calculations were studied in detail [8]. The clusters look like a fullerene, but have the internal core. In this region of sizes, the structure of clusters of minimal energy is characterized by a well-coordinated close-packed atomic arrangement, whereas the clusters of 10–30 atoms are oblong in structure [9].

The optical absorption spectra of the Si clusters look like the spectra of bulk crystalline silicon [10]. However, it is assumed that, for the Si clusters, the transition to the structure of macrocrystal occurs in the region of sizes of 100 atoms and larger [11].

The structure and kinetic properties of the Si_{480} nanoparticle were studied in the temperature range between 600 and 2000 K [12] by the MD method, with Stillinger–Weber's (SW) potential [13]. The authors of [13] assume that the core structure of the nanoparticle is similar the structure of bulk vitreous silicon and the coefficient of self-diffusion of atoms in the nanoparticle at high temperatures is comparable to the similar characteristics of liquid silicon. Interaction between the Si atoms via the SW potential specifies the melting temperature of crystalline silicon at $T_m = 1691$ K [14]. This value of T_m is in better agreement with the experimental melting point (1685 K) than the value of T_m deduced from other empirical potentials and even from the ab initio calculations [15]. The studies of larger Si particles instead of smaller ones is important for microelectronics as well as for the development of the procedure of fabrication of nonsintering spherical nanoiparticles by chemical vapor deposition. We refer to a solid state as an amorphous state if it is reached through bypassing the liquid state, and as a vitreous state if the nonequilibrium solid state is attained by quick overcooling of the liquid.

The purpose of this study is to analyze the stability of vitreous and amorphous silicon nanoparticles 300–500 atoms in size when heated from the temperature $T = 300$ up to 1700 K, and to determine the heating-induced changes in their structural and kinetic properties.

2. POTENTIAL FUNCTIONS FOR COVALENT BONDS

Since the electron orbits often belong to several atoms simultaneously, the force acting on every atom is a many-particle force. In [13], Stillinger and Weber suggested that the total potential energy can be written as

$$U = \sum_{j<j} \Phi_{(2)}(r_{ij}) + \sum_{i<j<k} \Phi_{(3)}(\mathbf{r}_i, \mathbf{r}_j, \mathbf{r}_k), \qquad (1)$$

where the pair potential of interaction is defined as

$$\Phi_{(2)}(r_{ij}) = \left[\frac{A}{r_{ij}^p}\exp\left(\frac{C}{r_{ij}-a}\right) - \frac{B}{r_{ij}^q}\exp\left(\frac{D}{r_{ij}-a}\right)\right]$$

if $r_{ij} < a$, and $\Phi_{(2)}(r_{ij}) = 0$ otherwise. Here, $r_{ij} = |\mathbf{r}_j - \mathbf{r}_i|$ is the spacing between atoms i and j located at the points $\mathbf{r}_i$ and $\mathbf{r}_j$, and A, B, C, D, p, q, and a are parameters.

The three-particle potential in Eq. (1) can be represented as

$$\Phi_3(\mathbf{r}_i, \mathbf{r}_j, \mathbf{r}_k) = h(\mathbf{r}_{ij}, \mathbf{r}_{ik}, \Theta_{jik}) + h(\mathbf{r}_{ji}, \mathbf{r}_{jk}, \Theta_{ijk}) + h(\mathbf{r}_{ki}, \mathbf{r}_{kj}, \Theta_{ikj}),$$

where Θ_{jik} is the angle formed by the vectors $\mathbf{r}_{ij} \equiv \mathbf{r}_j - \mathbf{r}_i$ and $\mathbf{r}_{ik} \equiv \mathbf{r}_k - \mathbf{r}_i$ at the vertex $\mathbf{r}_i$. The function commonly used to represent h is defined as

$$h(\mathbf{r}_{ij}, \mathbf{r}_{ik}, \Theta_{jik}) = \begin{cases} \lambda \exp\left(\frac{\gamma}{r_{ij}-a} + \frac{\gamma}{r_{ik}-a}\right)\left(\cos\Theta_{jik} + \frac{1}{3}\right), & r_{ij}, r_{ik} < a \\ 0 \quad r \geq a, \end{cases}$$

where λ and γ are parameters. The positive values of λ allow for reducing the tetrahedral-packed system of atoms to a more stable structure. The parameter Θ characterizes the deformation of bonds. We have $\Phi_{(3)} = 0$, if the angle Θ is perfectly tetrahedral, i.e., if $\cos\Theta = -1/3$. The SW potential allows us to describe the set of strains more accurately than can be done with the potentials of only two-particle interactions. The result of comparison of the van der Waals pair interactions with the interactions responsible for covalent bonding suggests that the latter interactions are between 10 and 100 times stronger than the van der Waals interactions. In spite of the high strength, it is impossible to describe the anisotropy of the material only by pair interactions. Hybridization of atoms provides the preferential directions of bonds. The i–j and i–k bonds of atom i form the valence angle φ. In the case of silicon and carbon that show the sp^3 hybridization, the valence angle is $\varphi = 109.47°$, whereas for the sp^2-hybridized carbon, the valence angle is $\varphi = 120°$. The appropriate potentials provide an increase in energy if the angle φ deviates from the equilibrium angle.

3. CALCULATION PROCEDURE

The simulation of the structure is carried out for the Si nanoparticles containing 300, 400, and 500 atoms. In the simulation, we use the SW potential. In the preliminary computer experiment, two types of Si_n nanoparticles with a noncrystalline atomic arrangement were obtained [16, 17]. One type refers to the vitreous nanoparticle formed as a result of quick cooling of a liquid Si particle from 3000 down to 300 K; the other type refers to the amorphous Si nanoparticle, in which the initial atomic arrangement was specified by a random-number generator and then the structure was relaxed at $T = 300$ K.

Here, the calculations were performed starting with the temperature of 300 K. The equations of motion were integrated numerically, following Verlet's procedure, one of the most stable procedures. This procedure allows the temperature in the model to be controlled with a rather good accuracy. The time step Δt was 10^{-16} s. After every 1.02×10^6 time steps, the temperature of the nanoparticles was increased by 100 K by scaling the velocities of atoms appropriately within the interval $2 \times 10^4 \Delta t$. Then, within the time interval $10^6 \Delta t$, we calculated the physical and chemical characteristics of the nanoparticles. The average length of the Si–Si bond, $\langle L_b \rangle$, and the average number of bonds per atom, $\langle n_b \rangle$, were determined by constructing the Voronoi polyhedrons (VPs). The VPs were constructed every 1000 time steps for 200 atoms located closer to the center of mass of the nanoparticle. Among the nearest neighbors established by constructing the VPs, we selected the atoms that were spaced by a distance no larger than 0.3 nm. This value is close to the parameter in the Morse potential [18] that describes the Si–Si interactions.

To analyze the physical properties of the nanoparticles in detail, we assumed the nanoparticles to be spheres divided into concentric layers of equal thickness d. The first layer was considered as a sphere whose radius was four times larger than d. The centers of the spheres and concentric layers coincided with the center of mass of the nanoparticles. The number of atoms in each spherical layer was determined in every $10\Delta t$. In the same time intervals, the potential energy and the mobility coefficients for atoms in each layer were calculated. The difference between the number of atoms in the layers was no larger than 40. A better idea of the state of the layers can be gained from the relative excess potential energy defined as

$$\Delta U / \langle U \rangle = (U_n - \langle U \rangle) / \langle U \rangle,$$

where U_n is the potential energy of the atoms involved in the nth layer and $\langle U \rangle$ is the average potential energy of the nanoparticle. The layers were numbered from the center of the nanoparticle.

The total mobility coefficient was calculated in terms of the atomic mean-square displacements, according to the expression [19]

$$D = \lim_{t \to \infty} \frac{1}{6t} \frac{1}{N} \sum_{i=1}^{N} [\mathbf{r}_i(t + t_0) - \mathbf{r}_i(t_0)]^2,$$

where $\mathbf{r}_i(t)$ is the radius vector of the ith atom at a time t. The atomic displacements in a spherical nanoparticle can be represented [19] by two components, the radial component $\langle (\Delta \mathbf{r})^2 \rangle_r$, which characterizes the displacements of atoms to or from the center of the nanoparticle; and the tangential component $\langle (\Delta \mathbf{r})^2 \rangle_t$, which describes the displacements orthogonal to the radial direction. Thus, we have

$$D_r = \frac{1}{6} \lim_{t \to \infty} \frac{\langle r^2(t) + r^2(0) - 2r(t)r(0) \rangle}{t},$$

$$D_t = \frac{1}{6} \lim_{t \to \infty} \frac{\langle r(t)r(0)[2 - 2\mathbf{u}(t)\mathbf{u}(0)] \rangle}{t}.$$

Here, $\mathbf{u} = \mathbf{r}(t)/|\mathbf{r}(t)|$ is the unit vector. The coefficients D_r and D_t characterize the radial and tangential components of the mobility of atoms in the nanoparticles. We calculated the radial distributions of these quantities averaged over the concentric layers of a spherical nanoparticle. Since $\langle (\Delta \mathbf{r})^2 \rangle = \langle (\Delta \mathbf{r})^2 \rangle_r + \langle (\Delta \mathbf{r})^2 \rangle_t$, the mobility coefficients are interrelated by the expression $D = D_r + D_t$.

4. CHARACTERISTICS OF THE Si–Si BOND

In Fig. 1, the atomic arrangements in the vitrified and amorphous Si_{400} nanoparticles at the temperature 1700 K are compared. The vitreous Si nanoparticle has a dense core and a friable outer layer that covers the major part of the core. The amorphous nanoparticle is larger in volume than the vitreous particle of the corresponding size. In the amorphous particle, the atoms are distributed more uniformly throughout the volume; however, in this case, the density in the outer region is lower than that in the core. Thus, in the radial direction from the center to the surface, there is a negative density gradient in the nanoparticles.

From the spread of the first peak of the radial distribution function (RDF), we can estimate the range of variations in the average bond length $\langle L \rangle$. The value of $\langle L \rangle$ determined in such manner for the inner part of the Si_{480} particle at 2060 K is in the range from 0.210 to 0.345 nm [12]. From the first peak of the RDF, it is found that, as the temperature is increased from 650 to 2060 K, the average coordination number varies from 4.6 to 8.5 for the inner part of the Si_{480} particle and from 3.2 to 3.7 for the surface atoms. The average bond length can be determined more exactly by constructing the VPs.

We now compare the average bond length $\langle L_b \rangle$ and the average number of bonds $\langle n_b \rangle$ per atom for vitrified and amorphous silicon nanoparticles, as found in the above manner. In the temperature region under consideration, the quantity $\langle L_b \rangle$ for the vitreous Si nanoparticle is no larger than 0.242 nm; for the amorphous Si nanoparticle, $\langle L_b \rangle$ is no larger than 0.247 nm. For the Si macrocrystal, $\langle L_b \rangle$ is 0.235 nm [20]. As the temperature is changed from 300 to 1700 K, the value of $\langle L_b \rangle$ averaged over the vitreous nanoparticles decreases by 0.5%. For the amorphous nanoparticles, the decrease is 0.2%. In the temperature region under consideration, the quantity $\langle n_b \rangle$ changes from 2.77 to 3.77 for the vitreous nanoparticles and from 2.56 to 3.50 for the amorphous nanoparticles. For the perfect Si macrocrystal, this quantity is $\langle n_b \rangle = 4$. With increasing temperature, the

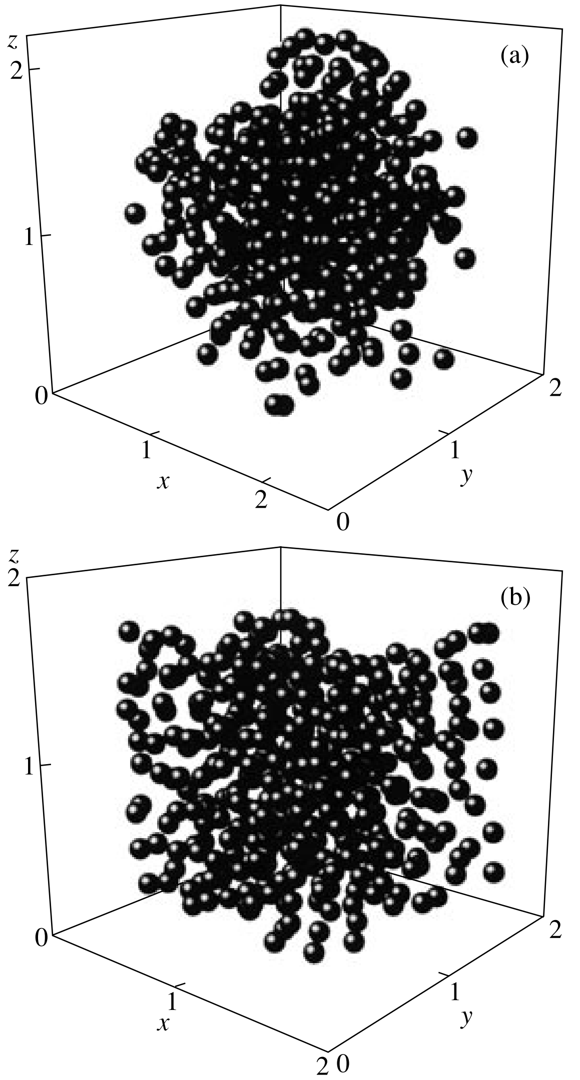

Fig. 1. Atomic arrangement in the Si_{400} nanoparticles at the temperature 1700 K: (a) vitreous silicon and (b) amorphous silicon. The coordinates of the constituent Si atoms, x, y, and z, are expressed in nanometers.

value of $\langle n_b \rangle$ averaged over the nanoparticles increases more steeply for the vitreous nanoparticles than for the amorphous ones. In the major part of the temperature region under consideration, the quantity $\langle n_b \rangle$ for the Si_{500} nanoparticle is larger than the same quantity for the Si_{300} and Si_{400} nanoparticles.

We now consider the temperature variations in the quantities $\langle L_b \rangle$ and $\langle n_b \rangle$ in more detail on the example of the Si_{400} nanoparticles. The temperature dependence of the average Si–Si bond length in the nanoparticles shows the oscillatory behavior (Fig. 2a). With increasing temperature from 300 to 1700 K, the quantity $\langle L_b \rangle$ increases by 0.08% for the vitreous Si_{400} nanoparticle and by 0.58% for the corresponding amorphous nanoparticle. We can see the tendency for an increase in the average number of Si–Si bonds per atom in the nanoparticles with increasing temperature (Fig. 2b). For the vitreous Si_{400} nanoparticle, the value of $\langle n_b \rangle$ increases by 17% as temperature is increased from 300 to 1700 K, and for the similar amorphous nanoparticle, $\langle n_b \rangle$ increases by 14%. It is worth noting that the number of bonds per atom in the vitreous Si nanoparticles is larger than the value of $\langle n_b \rangle$ in the corresponding-sized amorphous Si nanoparticles. This difference predetermines the higher stability of the vitrified nanoparticles at high temperatures.

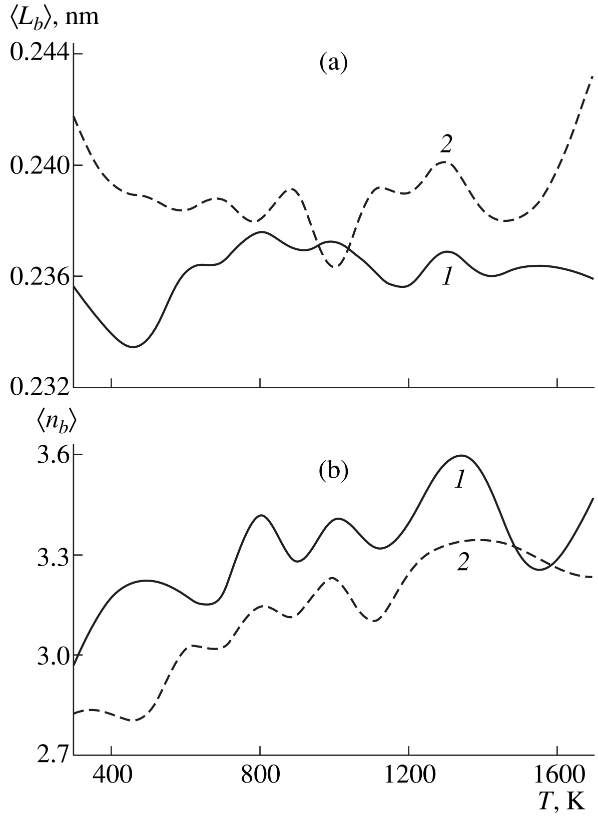

Fig. 2. The temperature dependence of (a) the average Si–Si bond length and (b) the average number of bonds per atom for the Si_{400} nanoparticle in (*1*) the vitrified state and (*2*) the amorphous state.

5. EXCESS POTENTIAL ENERGY IN NANOPARTICLES

In general, the energy E_b per bond decreases with increasing temperature for all nanoparticles under consideration. In the case of the vitreous Si_{300} nanoparticle, the value of E_b is somewhat smaller than E_b for the other two types of nanoparticles. The smallest value of E_b (–1.41 eV) is obtained for the vitreous Si_{300} nanoparticle at $T = 1100$ K, and the largest value of E_b (–1.01 eV) is obtained for the amorphous Si_{500} particle at 300 K. The ab initio calculations for the Si_2 dimer yield $E_b = -1.56$ eV; with $\langle n_b \rangle = 3$ for the cluster of ten atoms (Si_{10}), $E_b = -1.27$ eV [21].

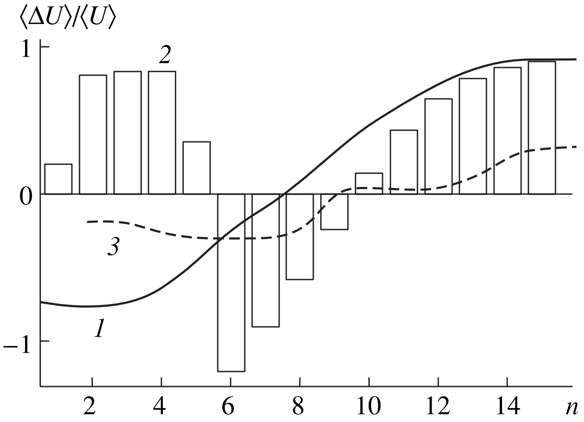

Fig. 3. The relative excess potential energy of the concentric layers (*1*, *2*) in the vitreous Si_{500} nanoparticle at the temperature (*1*) 300 and (*2*) 1700 K and (*3*) in the Ni_{188} nanocrystal at 300 K. The concentric layer number is denoted by *n*. The layers are numbered from the center of mass of the nanoparticle.

The energy state of a nanoparticle is most clearly represented by the profile of the relative excess potential energy. It is found that this profile is of the same type for the amorphous and vitreous nanoparticles. At the temperature 300 K, the excess potential energy smoothly changes from negative values in the inner regions of the nanoparticles to positive values in the outer regions. Curve *1* in Fig. 3 shows the dependence $\Delta U/\langle U\rangle = f(n)$ for the vitreous Si_{500} nanoparticle at $T =$ 300 K. The dependence $\Delta U/\langle U\rangle = f(n)$ for the Ni_{188} nanocrystal at 300 K [22] is also shown (curve *3*); this nanocrystal has a spherical void in the center. The initial size of the void corresponded to the volume of a fragment of 13 atoms of the face-centered cubic Ni crystal. The inner layers adjacent to the void are characterized by lager values of ΔU than the adjoining layers most distant from the center of the nanocrystal. The transition from $\Delta U < 0$ in the inner layers to $\Delta U > 0$ in the outer layers is more gradual for the Ni nanoparticles than that for the Si nanoparticle. An increase in the kinetic energy of the nanoparticles induces a redistribution of the potential energy in the constituent concentric layers. For the nanoparticles under study, the number of concentric layers with the energy U_n lower than the average energy of the particle, $\langle U\rangle$ is eight or nine, and the number of layers with $U_n > \langle U\rangle$ is six or seven.

We now consider in more detail the behavior of the function $\Delta U/\langle U\rangle = f(n)$ for the vitreous Si nanoparticles. In the case of the Si_{500} particle at $T = 1700$ K, this function is shown by bar chart *2* in Fig. 3. The energy strain appears even at T = 500K. In this case, the first five inner concentric layers in the Si_{500} nanoparticle have the energy $U_n > \langle U\rangle$. A similar relation between the energies is found for the first six layers in the Si_{300} and Si_{400} nanoparticles. The next four concentric layers (middle layers) in the nanoparticles have energy lower than $\langle U\rangle$. The six outer layers of the Si_{500} nanoparticle retain the energy $U_n > \langle U\rangle$. The same relation between the energies U_n and $\langle U\rangle$ is found for the five outer layers in the Si_{300} and Si_{400} nanoparticles. The distribution of the quantity $\Delta U/\langle U\rangle$ among the concentric layers of the clusters remains close to the above-considered distribution at $T = 1700$ K as well. In this case, for the Si_{500} nanoparticle, the lowest energy is characteristic of the sixth layer (Fig. 3, bar chart *2*); for the Si_{300} and Si_{400} nanoparticles, the lowest energy corresponds to the eighth layer. The most substantial difference in energy between two adjacent layers in the Si_{500} nanoparticle is found for the fifth and sixth concentric layers. The highest energy is inherent in the 15th outer layer. Thus, for the Si nanoparticles heated up to temperatures 500 K and higher, the energetically more preferential region is in the middle spherical layer involving four layers obtained above by dividing the spherical nanoparticle into concentric layers.

6. KINETIC PROPERTIES

For dispersed particles in the solid state, we can recognize three basic types of diffusion: surface diffusion, bulk diffusion, and diffusion over the grain boundaries. Theoretical calculations show that, if there is no oxide surface layer, surface diffusion controls the mechanism of coalescence of silicon nanoparticles in the temperature range from 1273 to 1573 K [23]. The other most active mechanism of coalescence is diffusion over the grain boundaries; however, the efficiency of this mechanism is eight orders of magnitude lower compared to surface diffusion. Surface diffusion in stable nanoparticles is defined by the coefficient D_t. The kinetically stable state of a nanoparticle is defined by the relation $D_t > D_r$. This inequality means that the forces responsible for the surface tension dominate over the forces that tend to break down the particle. At the temperature 300 K, the radial component of the mobility coefficient is larger for the inner spherical layers. This feature is better pronounced for the vitreous nanoparticles and even more so for the nanoparticles bigger in size. For the amorphous Si nanoparticles, the components D_t and D_r in the concentric layers are comparable even at low temperatures ($T \leq 500$ K). It is found that, with increasing temperature, the mobility of atoms in the radial direction is enhanced for the outer concentric layers in the nanoparticles, while the motion of this type in the inner layers is suppressed. For the vitreous Si nanoparticles at $T = 1000$ K, the largest values of D_r are found for the 10th or 11th layers in the Si_{300} and Si_{400} nanoparticles and for the 13th layer in the Si_{500} particle. For the amorphous Si nanoparticles at this temperature, the components D_r and D_t in the spherical layers begin to become comparable. For these nanoparticles, the larger values of D_r and D_t in the surface region compared to the values in the other layers are of interest. At temper-

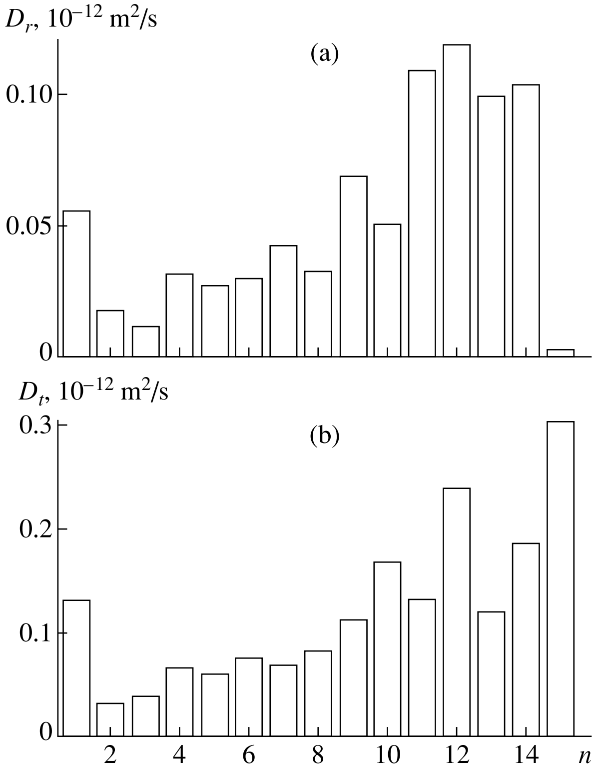

Fig. 4. The (a) radial and (b) tangential components of the atomic mobility coefficient D for the concentric layers in the vitreous Si_{500} nanoparticle at T = 1700 K.

atures around 1700 K, radical changes in the distributions $D_r(n)$ and $D_t(n)$ can be seen for the vitreous Si nanoparticles, especially for the Si_{500} particle (Fig. 4). The average value of the radial component of the mobility coefficient D for the outer (15th) layer increases by a factor of 8.8 for the Si_{300} nanoparticle and by a factor of 2.6 for the Si_{400} nanoparticle. In contrast, for the Si_{500} nanoparticle, the value of D_r for the 15th layer decreases by a factor of 10 in comparison with the corresponding value of D_r at 1000 K; at the same time, the maximum of D_r is shifted to the 12th layer (Fig. 4a). The other four outer layers (with the numbers from 11 to 14) are characterized by values of D_r noticeably larger than D_r for the remaining layers.

The tangential component of the mobility coefficient varies with temperature in a fairly similar manner. The specific feature of the behavior is that the increase in D_t in the outer layers with increasing temperature is more pronounced for the vitreous nanoparticles of larger size (Si_{400} and Si_{500}). For example, at T = 1700 K, the tangential component of the mobility coefficient D is prevailing in the 15th concentric layer for the Si_{400} and Si_{500} nanoparticles (Fig. 4b), and in the 13th layer for the Si_{300} particle. However, even in the deepest (first) layer in the vitreous nanoparticles, the value of D_t at T = 1700 K is three times larger than the corresponding value at T = 300 K. Averaged among the particles, the mobility coefficient D in the outer layer at T = 1700 K is 0.37×10^{-12} m^2/s. The experimental value of the coefficient of self-diffusion in liquid silicon at this temperature is 0.64×10^{-12} m^2/s [24]. The substantial increase in the components D_r and D_t for the outer layers in the vitreous nanoparticles suggests that a liquid surface layer is formed as the temperature approaches the melting point. The same trend is also evident for the amorphous nanoparticles, even at T = 1500 K. However, in this case, there are some specific features. The values of D_r and D_t for the outer layer are more than two times larger than the corresponding values for the other layers. The large value of D_t for the 15th layer suggests that a liquid outer layer appears; at the same time, the large value of D_r for this layer suggests that the amorphous nanoparticles are kinetically unstable. Thus, in the temperature region of melting, we find that the amorphous Si nanoparticles are kinetically unstable, whereas the vitreous Si nanoparticles involve a more stable outer liquid layer.

7. CONCLUSIONS

The results of this study show that the physical and chemical properties of the Si nanoparticles subjected to high-temperature heating depend on the procedure of fabrication of the particles. Therefore, the particular technology of production of the nanomaterials should be selected with reference to the field of application. Vitreous Si nanoparticles can be used under high-temperature conditions, since these particles are thermally more stable than similar-sized amorphous particles. In the region of the transition to melting, the behavior of the average bond length, $\langle L_b \rangle$, and the average number of bonds per atom, $\langle n_b \rangle$, depends on the procedure of fabrication of the nanoparticle and on its size. Only at temperatures below 500 K do the vitreous Si nanoparticles feature a more gradual variation in the radial profile of the excess potential energy that changes from low energies inside the nanoparticle to high energies at its surface. Due to the thermally induced strains, this profile is v-like in shape. The state of the thermally strained nanoparticles is typified by the presence of spherical layers radically different in energy. The inner and outer layers of the heated nanoparticle feature an excess potential energy relative to the average energy $\langle U \rangle$. The middle spherical layer is characterized by very low potential energies. For a number of atoms in this layer, the energy U is two times lower than $\langle U \rangle$.

The vitreous nanoparticles melt in the temperature range from 1500 to 1700 K. This transition is identified by the substantial increase in the atomic mobility coefficient D and the approach of this characteristic to the coefficient D for liquid silicon. Computer simulation of the structure of the vitreous Si_{480} nanoparticles using the SW potential showed that, in this case, melting occurred near the temperature T^* = 1560 K [12]. The quantity T^* is the average temperature that characterizes the melting-temperature region. In the study reported here, it is shown that the division of the nanoparticle volume into concentric layers and the determination of the components of the mobility coefficient, D_r and D_t, for each layer provide a more adequate description of the thermally induced destruction of the nanoparticles, including the identification of the initial temperature for the melting region.

The onset of melting is identified from the behavior of the kinetic criterion of stability. According to this criterion, a nanoparticle can be characterized by the "liquid-like" behavior from the point at which atomic displacements in the radial direction begin to dominate over the corresponding displacements in the tangential direction. With increasing temperature, with a consequent rise in the density of the nanoparticle, a substantial increase in the radial displacements is evident only in the outer layers (in the outermost layer for the amorphous nanoparticles). As shown by the detailed analysis of the distributions of the radial component of the atomic-mobility coefficient among the concentric layers, the kinetic instability occurs at the temperature 1400 K for the amorphous Si nanoparticles and at 1500 K for the vitreous Si nanoparticles.

Thus, data on the stability of silicon nanoparticles are obtained. It is established that, at high temperatures, the differences between the vitrified and amorphous nanoparticles reveal themselves in their structural and, especially, kinetic properties. This should be taken into account in selecting the field of application of the nanoparticles.

ACKNOWLEDGMENTS

This study was supported by the Presidium of the Ural Division, Russian Academy of Sciences (an integrated project of the Ural Division and the Far-East Division, Russian Academy of Sciences).

REFERENCES

1. Y. Zhao, Y.-H. Kim, M.-H. Du, and S. B. Zhang, Phys. Rev. Lett. **93**, 015502 (2004).
2. Z. Chen, H. Jiao, G. Seifert, et al., J. Comput. Chem. **24**, 948 (2003).
3. K. Nishio, J. Koga, T. Yamaguchi, and F. Yonezawa, Phys. Rev. B **67**, 195304 (2003).
4. N.-M. Park, C.-J. Choi, T.-Y. Seong, and S.-J. Park, Phys. Rev. Lett. **86**, 1355 (2001).
5. B.-H. Kim, C.-H. Cho, T.-W. Kim, et al., Appl. Phys. Lett. **86**, 091908 (2005).
6. L. Pizzagalli, G. Galli, J. E. Klepeis, and F. Gygi, Phys. Rev. B **63**, 165324 (2001).
7. L. Mitas, C. Grossman, I. Stich, and J. Tobik, Phys. Rev. Lett. **84**, 1479 (2000).
8. U. Rothlisberger, W. Andreoni, and M. Parrinello, Phys. Rev. Lett. **72**, 665 (1994).
9. Y. Kawazoe, T. Kondow, and K. Ohno, *Clusters and Nanomaterials. Theory and Experiment* (Springer, Berlin, 2002), Chap. 2, p. 57.
10. K.-D. Rinnen and M. L. Mandich, Phys. Rev. Lett. **69**, 1823 (1992).
11. K. Efrajani, Y. Hashi, K. Shida, and Y. Kawazoe, *Computational Modeling and Simulation of Materials*, Ed. by P. Vincenzini and A. Degli Esposti (Techna Srl, Tokyo, 1999), Chap. 1, p. 15.
12. M. R. Zachariah, M. J. Carrier, and E. Blaisten-Barojas, J. Phys. Chem. **100**, 14856 (1996).
13. F. H. Stillinger and T. A. Weber, Phys. Rev. B **31**, 5262 (1985).
14. C. R. Miranda and A. Antonelli, J. Chem. Phys. **120**, 11672 (2004).
15. O. Sugino and R. Car, Phys. Rev. Lett. **74**, 1823 (1995).
16. A. E. Galashev, V. A. Polukhin, I. A. Izmodenov, and O. A. Galasheva, Poverkhnost: Rentgen. Sinkhrotron. Neĭtron. Issled., No. 1, 41 (2006).
17. A. E. Galashev, V. A. Polukhin, I. A. Izmodenov, and O. R. Rakhmanova, Fiz. Khim. Stekla **32**, 99 (2006) [Glass Phys. Chem. **32**, 99 (2006)].
18. J. D. Kubicki and A. C. Lasaga, Am. Mineral. **73**, 941 (1988).
19. C. L. Briant and J. J. Burton, Nature Phys. Sci. **243**, 100 (1973).
20. E. F. Sheka and E. A. Nikitina, Dokl. Akad. Nauk, Ser. Khim. **378**, 208 (2001).
21. M. Menon and K. R. Subbaswamy, Phys. Rev. B **47**, 12754 (2002).
22. A. E. Galashev, Poverkhnost: Rentgen. Sinkhrotron. Neĭtron. Issled., No. 1, 77 (2005).
23. S. H. Ehrman, M. I. Acuino-Class, and M. R. Zachariah, J. Mater. Res. **14**, 1664 (1999).
24. W. M. Robertson, J. Am. Ceram. Soc. **64**, 9 (1981).

Translated by É. Smorgonskaya